PHYSICAL REVIEW B VOLUME 2, NUMBER 5 1 SEPTEMBER 1970

Neutron Scattering in the Linear Chain Antiferromagnet $CsMnCl_3 \cdot 2H_2O$†

J. Skalyo, Jr., and G. Shirane
Brookhaven National Laboratory, Upton, New York 11973

and

S. A. Friedberg and H. Kobayashi*
Carnegie-Mellon University, Pittsburgh, Pennsylvania 15213

(Received 14 April 1970)

Highly unusual magnetic scattering of neutrons has been observed in $CsMnCl_3 \cdot 2H_2O$ ($T_N = 4.89$ °K). The scattering in reciprocal space occurs in *planes* of constant intensity at temperatures as high as $10T_N$. These planes are perpendicular to the a^* axis and peak strongly at h odd. This is the first observation of definitive evidence for linear antiferromagnetic chains. At approximately $2T_N$, the planes develop an intensity variation with peaks occurring in the vicinity of eventual magnetic Bragg peaks. The nature of the scattering here is indicative of long chains of spins becoming correlated in the remaining two dimensions through weak interchain coupling. The substance thereupon attains a three-dimensional ordering at T_N. The sublattice magnetization below T_N follows a power-law behavior in the range $0.0005 < (T_N - T)/T_N < 0.07$ with critical exponent 0.30.

I. INTRODUCTION

A considerable amount of experimental evidence suggests the existence of linear-chain antiferromagnets. These are generally substances which contain paramagnetic ions in a structure permitting a dominant superexchange mechanism to exist in one direction. Measurements of both the susceptibility and the heat capacity are characterized by broad maxima occurring at temperatures substantially above the temperature T_N at which interchain coupling causes long-range order to occur, usually in three dimensions. The large spin-entropy reduction accompanying the short-range linear-chain ordering leaves only a small λ anomaly in the heat capacity when long-range order is finally established at T_N.

These substances are especially interesting since theoretically tractable models[1-4] exist with which to compare the observations. Griffiths[5] has shown that both the heat capacity and susceptibility of $Cu(NH_3)_4SO_4 \cdot H_2O$ can be well fitted by expressions derived for long chains of antiferromagnetically coupled spins. The present work is concerned with $CsMnCl_3 \cdot 2H_2O$. The susceptibility in this case has been measured by Smith and Friedberg[6] and shown to exhibit pronounced independent linear-chain behavior down to temperatures of about $2T_N$ ($T_N \approx 4.89$ °K). The onset of long-range order above 0 °K indicates, of course, the presence of non-negligible interchain coupling which must be treated in any complete theory. While the good fits obtained with simple models are suggestive of the existence of linear chains, they do not constitute direct proof of such behavior.

A similar broad maximum well above T_N occurs in the susceptibility of substances which are two-dimensional antiferromagnets, e.g., K_2NiF_4. Here the superexchange paths are evident in only two directions from structural considerations. Definitive proof of two-dimensional character was first given by Birgeneau *et al.*[7] for K_2NiF_4, using neutron-scattering experiments. Similar experiments by Skalyo *et al.*[8] subsequently indicated two-dimensional behavior in $Mn(HCOO)_2 \cdot 2H_2O$. In the present work, we have utilized similar neutron-scattering methods to give the first concrete picture of the ordering which takes place in the linear-chain antiferromagnet $CsMnCl_3 \cdot 2H_2O$.

II. SAMPLE AND APPARATUS

$CsMnCl_3 \cdot 2H_2O$ was chosen for the present investigation because it possesses several desirable features. The Mn^{++} ion is in an ^6S state and exhibits a moment corresponding to $S = \frac{5}{2}$ and $g = 2.00$. This large moment ensures suitable neutron-scattering intensities (25 times better than copper). The Néel temperature is 4.89 °K with broad maxima occurring in both the susceptibility[6] and the heat capacity[9] above 20 °K. Thus, the linear-chain characteristics can be observed over a large temperature range, while the ordered state below T_N can be conveniently studied as well.

The crystal structure of $CsMnCl_3 \cdot 2H_2O$ has been determined by Jensen *et al.*[10] It is of the orthorhombic space group *Pcca* with four molecules in the chemical unit cell. The dimensions of the cell are 9.06, 7.285, and 11.455 Å for the a, b, and c directions, respectively. The magnetic structure

has been deduced by Spence *et al.*[11] using NMR. The space group is $P_{2b}c'ca'$ with the magnetic cell doubling the chemical cell in the b direction; confirmation of this structure is given by us in Sec. IV. The lower half of the magnetic cell is illustrated in a projection on the (001) plane in Fig. 1. The upper half of the cell is related by symmetry to the lower half and can be obtained by operating on the illustrated atomic positions with an a' glide plane perpendicular to the c axis.

Each Mn^{++} ion is surrounded by four Cl^- ions and two H_2O molecules which form a distorted octahedron. In Fig. 1 we see that two adjacent octahedra share a common Cl^- ion so that chains of the form Mn^{++}-Cl^--Mn^{++}-Cl^--Mn^{++} extended indefinitely in the a direction. The dominant superexchange coupling of Mn^{++} spins probably occurs along these chains. Interchain linkages between Mn^{++} spins in the b and c directions are possible only through several intermediate atoms. The intrachain separation of neighboring Mn^{++} ions is 4.56 Å, while the corresponding interchain distance is 7.29 Å.

Susceptibility measurements[6] in the paramagnetic region ($T > T_N$) can be accurately described by an independent linear-chain model with isotropic antiferromagnetic intrachain exchange, $J_1 = -3.0k$. As a consequence, presumably, of a weak interchain coupling, antiferromagnetic long-range order sets in below $T_N \approx 4.9\,^\circ$K with preferred spin alignment occurring along the b direction.[6] Oguchi[12] has pointed out the difficulty of incorporating such an additional interchain coupling into the model by the usual mean-field methods. Using the two-time temperature-dependent Green's-function technique,[13] he has obtained an approximate expression for T_N in terms of J_1 and an interchain exchange integral J_2. For $CsMnCl_3 \cdot 2H_2O$, one finds with this relation $J_2 \approx 0.01 J_1 = -0.03k$. Spence *et al.*[11] have extended this type of calculation to allow for possible differences in interchain coupling in the b and c directions. These, however, appear to be negligible.

It should be noted that the magnetic dipolar interaction between neighboring spins on adjacent chains is of the order of $S^2g^2\mu_B^2/d^3 \approx 0.02k$, taking $d = 7.3$ Å. Thus, it is quite possible that the interchain spin coupling in this material is largely, if not entirely, dipolar in character.

Single crystals of $CsMnCl_3 \cdot 2H_2O$ were grown by the slow evaporation of a saturated aqueous equimolar solution of CsCl and $MnCl_2 \cdot 4H_2O$. This was done at 30 °C to ensure the growth of the desired orthorhombic crystals. At lower temperatures, triclinic crystals of $Cs_2MnCl_4 \cdot 2H_2O$ are obtained. The present sample was a large bicrystal with dimensions 1.46, 0.9, and 0.4 cm along the a, b, and c directions, respectively. The two crystallites were misaligned by $\approx 0.35^\circ$ and each had a mosaic spread of 0.2°. This small misalignment presented no difficulties in the present experiment.

The neutron-scattering measurements were conducted on a double-axis spectrometer at the Brookhaven High Flux Beam Reactor. The (311) reflection of a germanium monochromator provided neutrons of wavelength 1.03 Å with no $\frac{1}{2}\lambda$ contamination. The collimation was 20 min before and after the sample. The sample was sealed in an aluminum holder in an atmosphere of helium gas. The latter was used to promote thermal equilibrium in the sample. The holder was mounted in a liquid-helium Dewar which could be attached to the goniometer of the spectrometer. The thermometer was mounted in a recess in the base of the holder in close proximity to the sample. A heater wound on the holder permitted the temperature to be controlled and maintained above the bath temperature which was regulated by a manostat. The sample temperature was regulated to within a few milli-

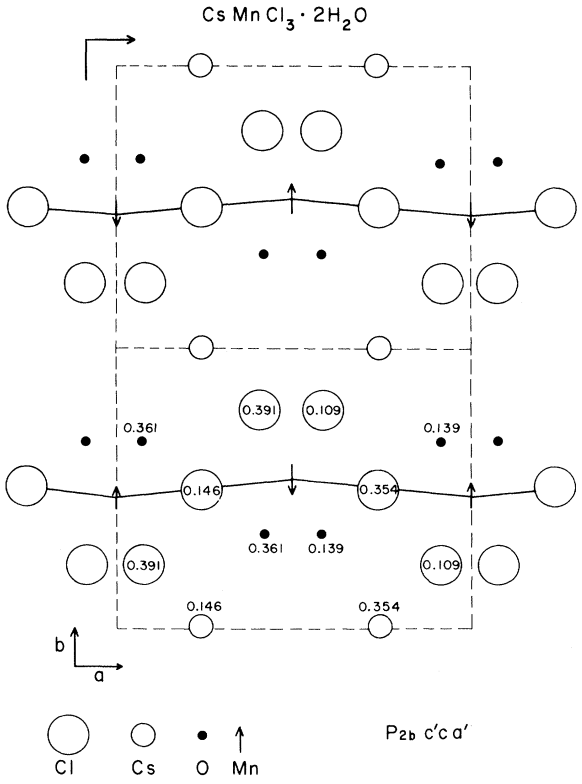

FIG. 1. (001) projection of the lower half of the magnetic cell of $CsMnCl_3 \cdot 2H_2O$. Upper half of the cell is obtained from lower half by summetry using the a' glide plane perpendicular to the c axis. Linear chains of antiferromagnetic spins are parallel to the a axis and are at the level $z = 0.25$.

degrees by an electronic servomechanism.

III. NEUTRON SCATTERING

In general,[14] the scattering of unpolarized neutrons by N localized magnetic spins is proportional to the space-time Fourier transform $\mathcal{S}^{\alpha\beta}(\vec{Q}, \omega)$ of the time-dependent two-spin correlation function $\langle S_0^\alpha(0) S_r^\beta(t) \rangle$. Using essentially the formalism of Ref. 14, the cross section may be written

$$\frac{d^2\sigma}{d\Omega' dE'} = A(\vec{k}, \vec{k}') \sum_{\alpha\beta} (\delta_{\alpha\beta} - \hat{Q}_\alpha \hat{Q}_\beta) \mathcal{S}^{\alpha\beta}(\vec{Q}, \omega), \quad (1)$$

where $\vec{k}$ and $\vec{k}'$ are the wave vectors of incident and scattered neutrons, respectively, and $\vec{Q} = \vec{k} - \vec{k}'$. For systems in which there is only exchange coupling, a contribution to the scattering occurs for $\alpha = \beta$ only. The scattering intensity can be written as the sum of two terms. The first is a magnetic Bragg peak contribution

$$\frac{d\sigma}{d\Omega'}\Big|_B = A(\vec{k}, \vec{k}) \frac{n^2}{N} \delta(\omega)\, \delta(\vec{G}_m - \vec{Q}) \times \sum_\alpha (1 - \hat{Q}_\alpha^2) \Big| \sum_{r'} e^{i\vec{Q}\cdot\vec{r}'} \langle S^\alpha(\vec{r}') \rangle \Big|^2 , \quad (2)$$

where $\vec{G}_m$ is a magnetic reciprocal-lattice point, n is the total number of magnetic unit cells, and the r' sum is over one magnetic unit cell.

The second term is an energy-dependent contribution. The double-axis spectrometer used in the present experiment counts neutrons of all energies in the direction $\hat{k}'$. If the initial neutron energy is large compared to the inelasticity of the magnetic scattering, the integration is approximately equal to an integration at constant $\vec{Q}$. If, in addition, the energy integration is primarily due to an energy range where $\hbar\omega \ll kT$, the scattering intensity can be written quasielastically as

$$\frac{d\sigma}{d\Omega'}\Big|_D = A(\vec{k}, \vec{k}) \sum_\alpha (1 - \hat{Q}_\alpha^2) \frac{S(S+1)}{3\chi_0} \chi^{\alpha\alpha}(\vec{Q}) . \quad (3)$$

Here χ_0 is the Curie-law susceptibility, and $\chi^{\alpha\alpha}(\vec{Q})$ are the diagonal elements of the wave-vector-dependent susceptibility tensor. If the spin correlation function is taken to be of the Ornstein-Zernike type, one finds

$$\chi^{\alpha\alpha}(\vec{Q}) \propto 1/(\kappa^2 + \vec{q}\cdot\vec{q}) \quad \text{with} \quad \vec{Q} = \vec{G}_m + \vec{q} . \quad (4)$$

The inverse correlation range parameter κ goes to zero at T_N for the parallel susceptibility and at somewhat less than T_N for the perpendicular susceptibility.

The preceding discussion of both the Bragg and the diffusive components of scattering considers the crystal to order in three dimensions. If, for some reason, long-range order occurred in only one or two dimensions the appropriate lattice sums would not result in the three-dimensional Bragg condition $\delta(\vec{G}_M - \vec{Q})$. In the one-dimensional case, the Bragg condition would occur with respect to planes in reciprocal space, while two-dimensional order gives a Bragg condition with respect to lines in reciprocal space. The three cases are shown descriptively in Fig. 2 for a simple antiferromagnetic structure. A similar alteration necessarily occurs also for the diffusive scattering. The form for $\chi^{\alpha\alpha}(\vec{Q})$ would hence be some function of $\vec{q}$ where $\vec{q}$ is measured from the magnetic reciprocal-lattice plane or line in one- or two-dimensional systems, respectively.

Fisher[1] gives an exact expression for $\langle S_i^z S_{i+j}^z \rangle$ in the case of the Heisenberg model for the linear chain in the classical $(S \to \infty)$ limit,

$$\langle S_i^z S_{i+j}^z \rangle = \tfrac{1}{3}[U(K)]^{|j|} ,$$

with

$$U(K) = (\coth K - 1/K) \quad \text{and} \quad K = J'/2kT . \quad (5)$$

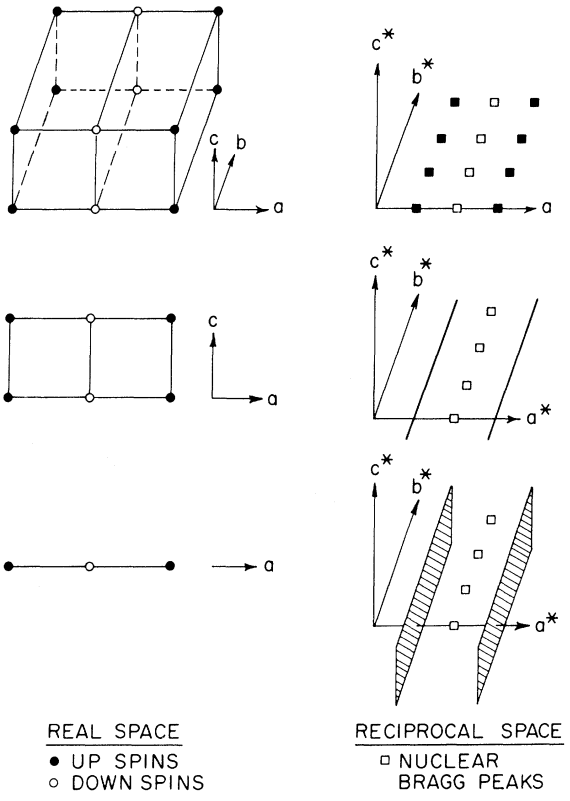

FIG. 2. Schematic representation of the type of Bragg scattering obtained for various kinds of order in a three-dimensional lattice. From top to bottom, we have three-, two-, and one-dimensional ordering with magnetic Bragg peaks, lines, and planes, respectively.

The neutron cross section in the case of an antiferromagnetic linear chain in this limit is proportional to the Fourier transform

$$\frac{d\sigma}{d\Omega'} \propto \lim_{N\to\infty} \sum_{j=-N}^{N} e^{ijQa/2}[U(K)]^{|j|}e^{ij\pi} \quad , \tag{6}$$

where $\frac{1}{2}a$ is the distance between adjacent spins and Q is the component of $\vec{Q}$ along the chain. Using the series expansion for $1/(1-x)$, one finds

$$\frac{d\sigma}{d\Omega'} \propto \frac{1+U(K)}{1-U(K)+[2U(K)/1-U(K)][1-\cos(\frac{1}{2}Qa+\pi)]} . \tag{7}$$

As $Q = 2\pi h/a$, the intensity will peak at odd values of h in reciprocal space. It should be noted that in a region near h odd the scattering intensity will appear Lorentzian.

In the present experiment, a comparison with the data will be made using an approximate solution of the Heisenberg $S = \frac{5}{2}$ antiferromagnetic Hamiltonian

$$\mathcal{H} = -2J\sum_{i=1}^{N} \vec{S}_i \cdot \vec{S}_{i-1} \quad .$$

This simply involves the replacement of J' by $4|J|S(S+1)$ in Eq. (5). Smith and Friedberg[6] have analyzed the susceptibility of $CsMnCl_3 \cdot 2H_2O$ and obtain in this approximation $J = -3.115k$. The neutron scattering can therefore be fitted by adjustment of the proportionality constant of Eq. (7). Note that at h odd the scattering intensity diverges as $1/T$ and hence the staggered susceptibility diverges as $1/T^2$. In the presence of anisotropic linear-chain exchange, [3] an exponential-like divergence would appear in the scattering intensity.

Most of the experimental scans were made near the a^* axis in reciprocal space. As a result, the measurements give intensities which are approximately proportional to $\chi_b + \chi_c$, where $\chi_b = \chi_{\parallel}$. A measure of both components has not been attempted with the present sample due to the small signals obtained. Ordinarily, one might expect $\chi_b \approx \chi_c$ well above T_N; however, we note that a diffusive $\chi_\perp$ was not observed above T_N in the two-dimensional crystal K_2NiF_4.[15]

IV. MAGNETIC SCATTERING

The magnetic structure of $CsMnCl_3 \cdot 2H_2O$, illustrated in Fig. 1, shows the linear chain to have a slight zig-zag with one Mn^{++} ion located at $(0, 0.467, \frac{1}{4})$ and the others in positions required by symmetry.[10] From Eq. (2), the spin structure $P_{2b}c'ca'$ is found to give nonzero magnetic Bragg-peak intensity only at values of $k = \frac{1}{2}n$, where n is an odd integer. The resulting formula can simplify into two cases as follows:

$$I_{hkl} \propto f^2(\vec{Q})\sin^2\alpha_{hkl}\sin^2 2\pi(0.033k),$$

h and l even, and

$$I_{hkl} \propto f^2(\vec{Q})\sin^2\alpha_{hkl}\cos^2 2\pi(0.033k) , \tag{8}$$

h and l odd, where α_{hkl} is the angle between $\vec{Q}$ and the spin direction, and $f(\vec{Q})$ is the magnetic form factor. The observations of reflections $(h, k, 0)$ and $(h, k, 2k)$ were found to be in substantial agreement with Eq. (8), confirming that the magnetic structure is actually $P_{2b}c'ca'$. Quantitative agreement was not sought since the beam-depletion corrections necessitated by the incoherent scattering from hydrogen were large.

The reciprocal lattice of $CsMnCl_3 \cdot 2H_2O$ is shown in Fig. 3. The planar character of the magnetic scattering was clearly established by scans at positions A and C. Measurements were made from 2.5 to 60 °K with planar scattering observed at h odd. Typical A scans are shown in Fig. 4 with similar results obtaining for scan C. The large background is due to the incoherent scattering of the hydrogen in the sample.

An accurate determination of line shape and thus of a correlation length is not possible due to the high background, but a reasonable estimate can be made for comparison with interchain correlations. Taking account of a spectrometer resolution of $0.055a^*$ in this type of scan, one obtains a correlation length of ≈ 120 Å at $15°K(3T_N)$. This value, of course, depends upon an inelasticity consistent with the derivation of Eq. (3).

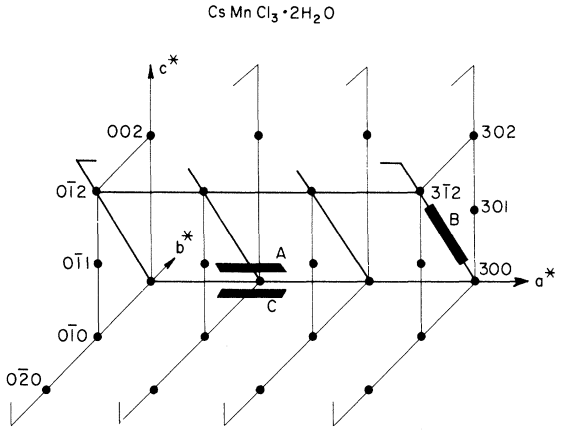

FIG. 3. Reciprocal space of $CsMnCl_3 \cdot 2H_2O$. Most of the scattering measurements were done in the zone containing (0, 0, 0), (3, 0, 0), and $(3, \bar{1}, 2)$. Planes of scattering due to the linear antiferromagnetic chain are perpendicular to a*. Scan A measured the intrachain correlations while interchain correlations were measured through the magnetic Bragg peak $(3, \frac{\bar{1}}{2}, 1)$ at scan B. Scan C in the [001] zone was performed to establish the planar character of the scattering.

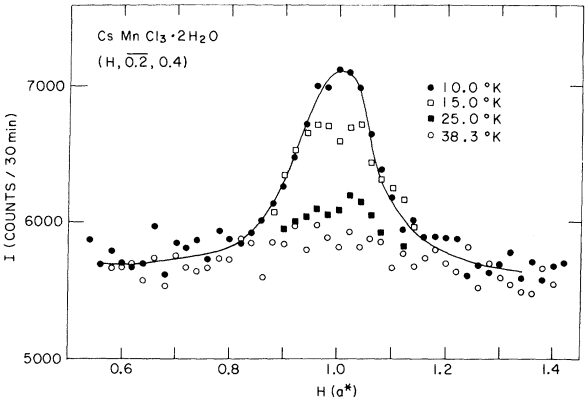

FIG. 4. Intrachain correlation measurements made at scan A. Note zero of the intensity scale is not shown.

The peak of the scan at $h = 1$ has been plotted in Fig. 5 as a function of temperature and the dashed curve has been fitted using Eq. (7). This curve would be proportional to the staggered susceptibility were it not for limitations of instrumental resolution and possible inelasticity. Qualitatively, it behaves as if it were diverging. It would be expected to diverge at 0°K were there no interchain effects present.

A study of the interchain effects was made at $(3, \frac{1}{2}, 1)$. Scans were made along the plane of scattering intensity. The position is depicted by the B scan of Fig. 3. Measurements were not made at the stronger magnetic peak $(1, \frac{1}{2}, 1)$ because the scan here would have entailed larger crystal rotations on the spectrometer. This would have made necessary beam-depletion corrections to the scattering due to the large hydrogen concentration and inopportune crystal shape.

B-type scans are illustrated in Fig. 6 for temperatures from 4.90 to 15.0 °K. The scan is observed to be quite flat at 15.0 °K, indicative of the immeasurably small interchain correlation at the temperature. Spectrometer resolution is extremely narrow for these scans and correlation-length estimates can be made directly. The scan is still fairly broad at 5.50 °K with an interchain correla-

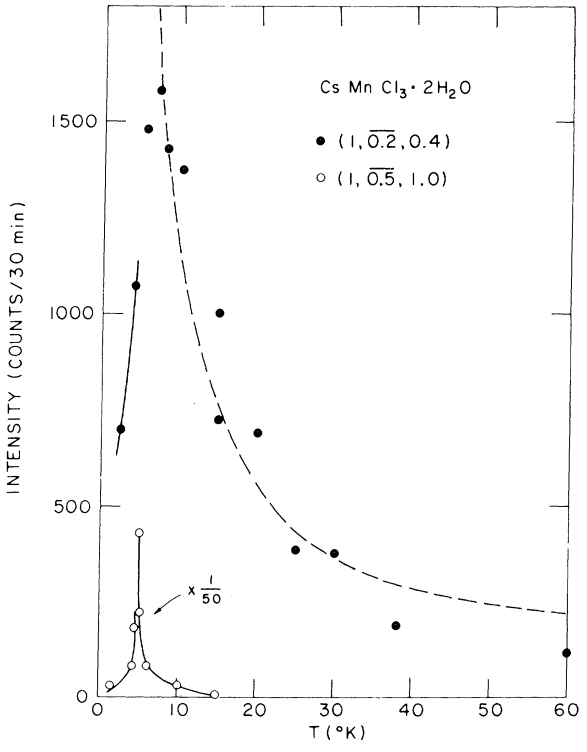

FIG. 5. Peak intensity of the A scans as a function of temperature. Much sharper temperature dependence occurring at $(1, \frac{1}{2}, 1)$ is given with $\frac{1}{50}$ of its intensity for comparison. The background has been subtracted. The dashed curve is a fit to Eq. (7).

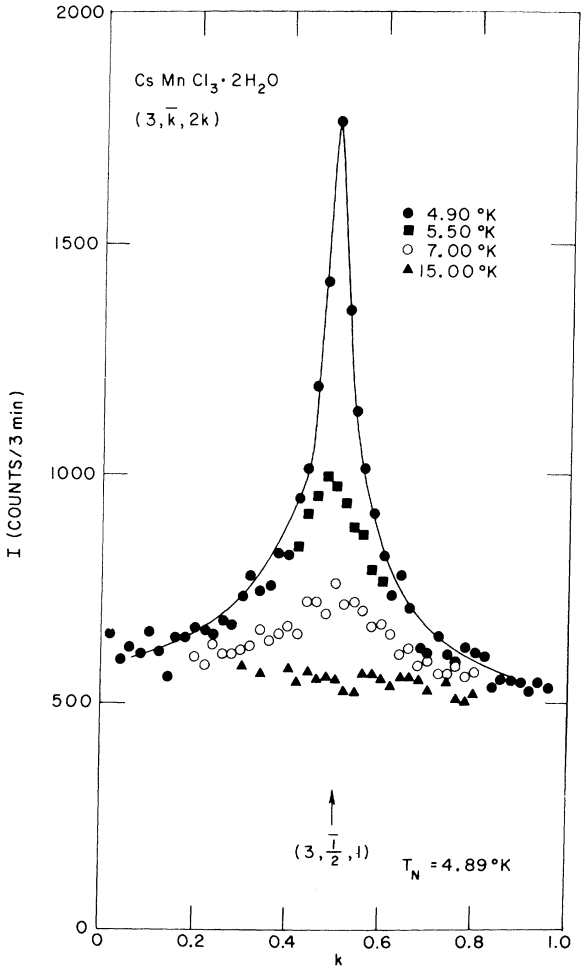

FIG. 6 Interchain correlation measurements made at scan B. Counting time here is 10 times less than in Fig. 4 due to the stronger intensities encountered.

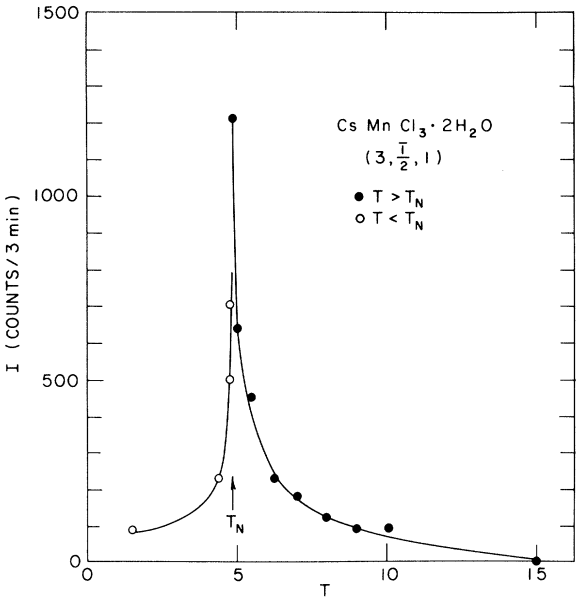

FIG. 7. Peak intensities of scan B at $(3, \frac{1}{2}, 1)$. The background has been subtracted.

tion length of $\approx$ 20 Å. Peak intensities of the B scans are shown in Fig. 7 as function of temperature from 1.5 to 15.0 °K. The same curves, suitably scaled, are shown in Fig. 5 for comparison with the intrachain component. The data of Fig. 7 clearly suggest a divergence at T_N.

V. MAGNETIZATION

The magnetic Bragg scattering of $S(\vec{Q}, \omega)$ is an elastic process and an expression of the cross section is given in Eqs. (2). Essentially, the intensity of the magnetic Bragg peaks is proportional to the square of the component of $\langle \vec{S} \rangle$ perpendicular to $\vec{Q}$. This term is thus zero above T_N and is proportional to the square of the magnetization below T_N. In the critical region "close" to the Néel point, the magnetization[16] is usually assumed to obey the power law

$$M(T) \propto (T_N - T/T_N)^{\beta} \quad . \tag{9}$$

It is therefore possible, in principle, to determine the critical index β by measuring the magnetic Bragg-peak intensity as a function of temperature.

We have seen in Sec. IV that the diffuse scattering persists below T_N and is superposed on the magnetic Bragg peak. The line shape of the diffuse scattering, however, is distinctly more extended in reciprocal space (i.e., note Fig. 6 where the Bragg peak would be only $\approx 0.02k$ wide at its base) and suitable corrections can be estimated by extrapolation.

Additional care must be taken to check the effect of extinction on the intensities. Preliminary measurements were therefore made at $(1, \frac{1}{2}, 1)$, $(3, \frac{1}{2}, 1)$, and $(5, \frac{1}{2}, 1)$ from 4.2 to 4.8 °K. The intensity ratios of the latter two peaks to that at $(1, \frac{1}{2}, 1)$ were independent of temperature. The $(5, \frac{1}{2}, 1)$ and $(3, \frac{1}{2}, 1)$ peaks are 10 and 2 times weaker than the $(1, \frac{1}{2}, 1)$ peak, indicating the absence of measurable extinction.

Detailed measurements of the magnetization were carried out at $(3, \frac{1}{2}, 1)$ over the range 1.500 to 4.890 °K and are shown in Fig. 8. The diffuse scattering was measured as a function of temperature and the corrections to the various Bragg intensities were obtained graphically. The correction is necessarily more important in the vicinity of the Néel point where the diffuse scattering is large and the magnetization is small. Typical reductions of the measured Bragg-peak intensities were 3 and 20% at 4.550 and 4.875 °K, respectively

The data were fitted by the method of least squares, the points being given weights inversely proportional to the measured intensity. The parameters of the fit were a scale factor, T_N and β; the method assumed perfect measurement of temperature. The weighted variance and the statistical distribution of errors with temperature were then compared for various fits which differed according to the included temperature range. For example, too wide a temperature interval extending out of the critical region resulted in a fit

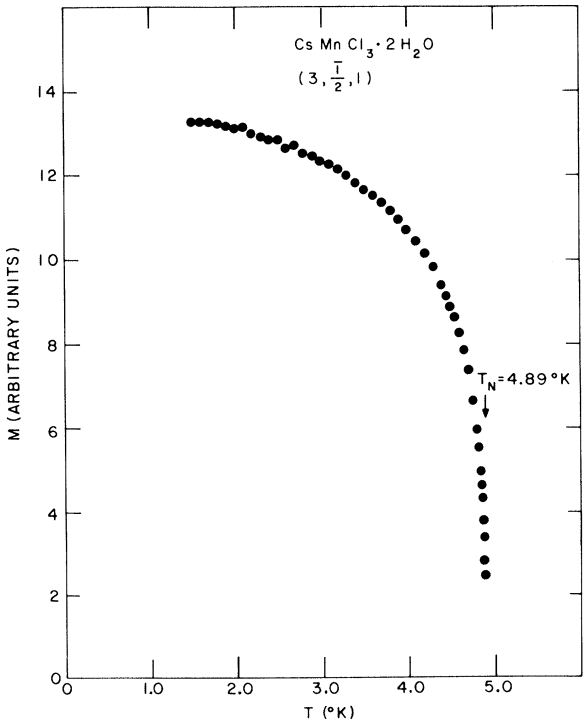

FIG. 8. Relative magnetization of $CsMnCl_3 \cdot 2H_2O$.

which gave positive deviations on the ends of the temperature range and negative deviations in the center. It was immediately evident that the critical range definitely did not persist below ≈ 4.55 °K.

As the lower bound of the temperature range was progressively increased to T_N from 4.55 °K, the values of the parameters did not change within their calculated standard deviations. The value of the weighted variance was about constant and the deviations appeared random. The best estimate was therefore made including all points above 4.55 °K and may be summarized in the formula

$$I(T) = A\left(\frac{T_N - T}{T_N}\right)^{2\beta},$$

where

$$A = 14270 \pm 600,\ T_N = 4.8925 \pm 0.001\ ^\circ\mathrm{K},$$

$$\beta = 0.30 \pm 0.01\ .$$

Utilizing data above 4.800 °K in the fit results in $T_N = 4.8930 \pm 0.0015$ °K and $\beta = 0.31 \pm 0.03$. The precision estimates given with the parameters mark out a region in parameter space where the true solution is 95% probable. The fit and the points are illustrated in Fig. 9.

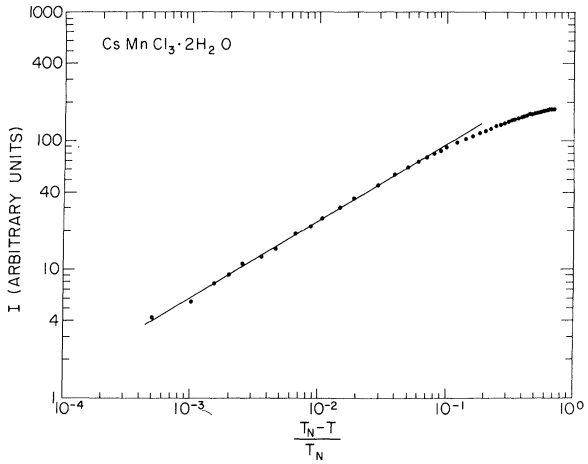

FIG. 9. Fit of the intensity of the magnetic Bragg peak $(3, \frac{1}{2}, 1)$ to the power law $(T_N - T/T_N)^{2\beta}$. The intensity is proportional to $\langle S^z \rangle^2$.

VI. CONCLUSIONS

Neutron-scattering measurements have been made on a linear-chain antiferromagnet and a qualitative picture obtained of the magnetization process. The crystal structure permits superexchange predominantly in the a direction and only very weak spin coupling perpendicular to the a axis. Therefore, the spin-system approximates one of isolated linear antiferromagnetic chains of spins. As such, the spin system exhibits correlations which extend over considerable distances as the temperature is lowered without achieving actual "long-range order." Above approximately $3T_N$, the system has acquired correlations in only one dimension. At $3T_N$ the average number of correlated spins within a chain is ≈ 25.

At approximately $2T_N$ the interchain interactions cause correlations to develop between the chains of correlated spins. The system orders three-dimensionally at T_N. The critical index $\beta(= 0.30)$ observed below T_N has essentially the value found for three-dimensional antiferromagnets with equal exchange coupling in the three directions ($J_1 = J_2 = J_3$). This is reminiscent of the behavior of two-dimensional Ising models for which the exact theory predicts $\beta = \frac{1}{8}$ regardless of the values of J_1 and J_2.[17,18]

The qualitative character of the picture given here should be noted. Measurements of both the A and B scans of Fig. 3 give approximately the combination $\chi_b + \chi_c$. An attempt to discern their individual behavior would require a much-improved signal. Thus, it is clearly desirable to perform measurements of this kind with a deuterated crystal of a suitable linear-chain antiferromagnet. The study of the dynamics of the spin system and a measurement of the inelasticity would also be much simplified. Measurements of this kind are planned.

The present results indicate that the scattering is in an approximate sense given by

$$\chi(\vec{q}) \propto [\kappa^2 + (a_1 q_x)^2 + (a_2 q_y)^2 + (a_3 q_z)^2]^{-1}\ , \qquad (10)$$

where the a_i are temperature dependent. The correlation length in any direction is then a_i/κ, with all three values of a_i diverging at T_N. At high temperatures $a_2 \approx a_3 \ll a_1$ giving the linear-chain behavior.

ACKNOWLEDGEMENTS

The authors would like to thank R. J. Birgeneau, M. Blume, H. Forstat, and V. J. Minkiewicz for illuminating discussions of linear-chain behavior.

†Work performed under the auspices of the U. S. Atomic Energy Commission, U. S. Office of Naval Research, and the National Science Foundation.

*On leave from Kyoto University, Kyoto, Japan.

[1]M. E. Fisher, Am. J. Phys. 32, 343 (1964).

[2]J. C. Bonner and M. E. Fisher, Phys. Rev. 135, A640 (1964).

[3]G. S. Joyce, Phys. Rev. Letters 19, 581 (1967).

[4]H. E. Stanley, Phys. Rev. 179, 570 (1969).

[5]R. B. Griffiths, Phys. Rev. 135, A659 (1964).

[6]T. Smith and S. A. Friedberg, Phys. Rev. 176, 660 (1968); the labels of the a and b axes are interchanged in

this reference.
[7]R. J. Birgeneau, H. J. Guggenheim, and G. Shirane, Phys. Rev. Letters 22, 720 (1969).
[8]J. Skalyo, Jr., G. Shirane, and S. A. Friedberg, Phys. Rev. 188, 1037 (1969).
[9]H. Forstat, J. N. McElearney, and N. D. Love (unpublished).
[10]S. J. Jensen and P. Andersen, Acta Chem. Scand. 16, 1890 (1962).
[11]R. D. Spence, W. J. M. de Jonge, and K. V. S. RamaRao, J. Chem. Phys. 51, 4694 (1969).
[12]T. Oguchi, Phys. Rev. 133, A1098 (1964).
[13]T. Oguchi and A. Honma, J. Appl. Phys. 34, 1153 (1963).
[14]For a review, see W. Marshall and R. D. Lowde, Rept. Progr. Phys. 31, 705 (1968).
[15]R. J. Birgeneau, J. Skalyo, Jr., and G. Shirane, J. Appl. Phys. 41, 1303 (1970).
[16]For a review, see M. E. Fisher, Rept. Progr. Phys. 30, 615 (1967).
[17]L. Onsager and B. Kaufman, Nuovo Cimento 6, 261 1949.
[18]C. H. Chang, Phys. Rev. 88, 1422 (1952).

PHYSICAL REVIEW B VOLUME 2, NUMBER 5 1 SEPTEMBER 1970

Extended Fine Structure in X-Ray Absorption Spectra of Certain Perovskites

Joseph Perel*

and

Richard D. Deslattes

National Bureau of Standards, Washington, D. C. 20234

(Received 9 July 1969)

In this paper we attempt to test the validity of the short-range-order (SRO) and the long-range-order (LRO) theories of the extended fine structure (EFS) in x-ray absorption spectra. This is done by comparing the EFS's of Ti, Ca, Zr, and Sr in the perovoskitelike compounds $SrTiO_3$, $CaTiO_3$, $SrZrO_3$, and $CaZrO_3$. The regularities which have been anticipated from SRO or LRO theories have not been observed. We are thus led to suggest that models are required other than those which have been used to explain the EFS.

I. INTRODUCTION

There is as yet no acceptable explanation of the extended fine structure (EFS) in x-ray absorption spectra. At present, two basically different theories attempt to explain this effect. The long-range-order (LRO) theory, introduced by Kronig,[1] attributes the EFS in crystals to the band structure of electronic energy levels. Qualitatively, this view correctly accounts for the relative displacements of the EFS extrema in crystallographically similar metals as well as for the similarity of EFS for the K edges of the components of certain binary compounds.[2]

Other experimental results are not easily reconciled with an LRO picture. The difficulty for an LRO-based theory of EFS is evidenced by the occasionally limited range of EFS (in some cases 50 eV or less[3]) and the more than occasional dissimilarities in the EFS for two elements in a compound. The latter becomes especially evident in this work. As may be inferred from the absence of any profile calculations in the literature, models of this class do not easily yield to quantitative treatment.

The other point of view, the short-range-order (SRO) theory,[4] is that the EFS exists primarily because the near neighbors of the absorbing atom influence the transition probability of the photoejected electron. Many features of the EFS which are believed to be capable of distinguishing between the two views are, on closer inspection, common to both. (For example, the dependence of the location of the characteristic absorption extrema on the inverse square of the dimensions of the cell is shared by SRO and LRO. Indeed this would follow even if the fine structure were due to recoil of the core electrons plus nucleus.) Qualitative successes for the SRO picture are found in the similarity of spectra in crystalline and amorphous phases, and in the component spectra of certain binaries.

Qualitative difficulties for a typical SRO-type description can be found in the spectra of polyatomic molecules, where this description should be applicable without reservation. It appears that in some cases[5] this expectation is realized, while in others[6] it is not. On the other hand, the SRO picture is readily quantified and has enjoyed semiquantitative agreement with experiment in a number of pure metals, albeit with the aid of some